Preclinical evaluation and validation of [F-18]HX4, a promising hypoxia marker for PET imaging

Preclinical evaluation and validation of [^{18}F]HX4, a promising hypoxia marker for PET imaging

Ludwig J. Dubois[a,1], Natasja G. Lieuwes[a], Marco H. M. Janssen[a], Wenny J. M. Peeters[b], Albert D. Windhorst[c], Joseph C. Walsh[d], Hartmuth C. Kolb[d], Michel C. Öllers[a], Johan Bussink[b], Guus A. M. S. van Dongen[c,e], Albert van der Kogel[b], and Philippe Lambin[a]

[a]Department of Radiation Oncology (MaastRO Lab), GROW–School for Oncology and Developmental Biology, Maastricht University Medical Centre, 6200 MD Maastricht, The Netherlands; [b]Department of Radiation Oncology, Radboud University Nijmegen Medical Centre, 6500 HB Nijmegen, The Netherlands; [c]Departments of Nuclear Medicine and PET Research, VU University Medical Centre, 1081 HV Amsterdam, The Netherlands; [d]Siemens Molecular Imaging Medical Solutions, Culver City, CA 90231; and [e]Department of Otolaryngology/Head and Neck Surgery, VU University Medical Centre, 1007 MB Amsterdam, The Netherlands

Edited by Michael E. Phelps, University of California, Los Angeles, CA, and approved July 21, 2011 (received for review February 16, 2011)

Hypoxia has been shown to be an important microenvironmental parameter influencing tumor progression and treatment efficacy. Patient guidance for hypoxia-targeted therapy requires evaluation of tumor oxygenation, preferably in a noninvasive manner. The aim of this study was to evaluate and validate the uptake of [^{18}F]HX4, a novel developed hypoxia marker for PET imaging. A heterogeneous accumulation of [^{18}F]HX4 was found within rat rhabdomyosarcoma tumors that was significantly ($P < 0.0001$) higher compared with the surrounding tissues, with temporal increasing tumor-to-blood ratios reaching a plateau of 7.638 ± 0.926 and optimal imaging properties 4 h after injection. [^{18}F]HX4 retention in normal tissues was found to be short-lived, homogeneous and characterized by a fast progressive temporal clearance. Heterogeneity in [^{18}F]HX4 tumor uptake was analyzed based on 16 regions within the tumor according to the different orthogonal planes at the largest diameter. Validation of heterogeneous [^{18}F]HX4 tumor uptake was shown by a strong and significant relationship ($r = 0.722$; $P < 0.0001$) with the hypoxic fraction as calculated by the percentage pimonidazole-positive pixels. Furthermore, a causal relationship with tumor oxygenation was established, because combination treatment of nicotinamide and carbogen resulted in a 40% reduction ($P < 0.001$) in [^{18}F]HX4 tumor accumulation whereas treatment with 7% oxygen breathing resulted in a 30% increased uptake ($P < 0.05$). [^{18}F]HX4 is therefore a promising candidate for noninvasive detection and evaluation of tumor hypoxia at a macroscopic level.

cancer | nuclear medicine | experimental research

The presence of hypoxic regions due to abnormalities in tumor vasculature, heterogeneously spread within solid tumors influences clinical outcome; as it is an independent predictor of poor prognosis-free survival in several types of cancer (1). In contrast, this unique tumor characteristic makes it an attractive target for novel drugs to increase the therapeutic effect of conventional cancer treatment modalities. Another approach is the use of intensity-modulated radiotherapy to give a higher dose to hypoxic areas while sparing the surrounding normal tissue (2, 3). Although treatments to counteract the negative effect of intratumoral hypoxia are under investigation, not all patients will benefit from such selective treatments. Therefore, to guide hypoxia-directed therapies in individual patients, it is important to evaluate tumor oxygenation using a reliable noninvasive method.

To date, a variety of methods are available for assessment of tumor oxygenation in solid tumors, of which polarographic oxygen electrodes and immunohistological assays remain the gold standard (4). These standard invasive modalities have not yielded reliable 3D images of the whole tumor for clinical use, and therefore research has been focused on noninvasive imaging techniques, such as positron-emission tomography (PET) using nitroimidazoles. The 2-nitroimidazole derivative fluoromisonidazole (FMISO) has been evaluated extensively for different cancer types (5–7). [^{18}F]FMISO PET imaging has evolved as the gold standard; however, clinical utility is limited, as there are concerns about the stability of the fluorine-18 linkage and the formation of metabolites in blood and urine. Furthermore, only modest signal-to-noise ratios are obtained due to its slow clearance, high lipophilicity, and liver and gut uptake (8). Second-generation, more water-soluble 2-nitroimidazoles, such as [^{18}F]-fluoroazomycin arabinoside ([^{18}F]FAZA) and [^{18}F]-fluoroerythronitroimidazole ([^{18}F]FETNIM), have been validated as hypoxia markers and have shown lower degradation resulting in higher tumor-to-background contrast (9, 10). On the other hand, more lipophilic fluorinated compounds, such as EF3, could be good alternatives for the detection of tumor hypoxia. However, in a comparative PET imaging study, we demonstrated no superiority of nitroimidazol-1H-yl-N-[^{18}F]-trifluoropropyl acetamide ([^{18}F]EF3) to [^{18}F]FMISO for the evaluation of hypoxia (11). Furthermore, it has been shown that the nonnitroimidazole hypoxia marker Copper(II)diacetyl-di(N^4-methylthiosemicarbazone) (Cu-ATSM) is selective for hypoxia in several tumor types. Clinical data obtained from non-small-cell lung cancer (NSCLC) patients demonstrated the feasibility of ^{60}Cu-ATSM imaging (12). However, uptake of ^{64}Cu-ATSM in fibrosarcoma-bearing mice correlated with vascular perfusion as opposed to hypoxia, and the accumulation did not decrease upon oxygenation using carbogen breathing (13). Tumor hypoxia response can also be evaluated by imaging of molecular markers of hypoxia, such as carbonic anhydrase IX (CAIX) using specific sulfonamides (14).

Alternatively, the 2-nitroimidazole nucleoside analog [^{18}F]HX4 was developed as a potential marker for hypoxic tumor cells. It represents a novel, click chemistry-based generation of derivatives in which structure–activity relationships, focused on the incorporation of a 1,2,3-triazole moiety, have been used to design an agent with preferred pharmacokinetic and clearance properties (15). Biodistribution and dosimetry studies in healthy monkeys and humans showed that the amount of unmetabolized [^{18}F]HX4 in blood and urine samples remained stable, liver and gastrointestinal tract uptake was relatively low, and the highest uptake of [^{18}F]HX4 was found in the urinary bladder, indicating an excretion primarily through the kidneys (15, 16). Because of the better water solubility and faster clearance, we hypothesized that

Author contributions: L.J.D., M.C.Ö., J.B., A.v.d.K., and P.L. designed research; L.J.D., N.G.L., M.H.M.J., W.J.M.P., A.D.W., and J.C.W. performed research; A.D.W., J.C.W., H.C.K., M.C.Ö., J.B., G.A.M.S.v.D., and A.v.d.K. contributed new reagents/analytic tools; L.J.D., N.G.L., M.H.M.J., W.J.M.P., J.C.W., J.B., and A.v.d.K. analyzed data; and L.J.D., N.G.L., M.H.M.J., and P.L. wrote the paper.

Conflict of interest statement: J.C.W. and H.C.K. are employed by Siemens Molecular Imaging Medical Solutions and therefore have a relationship with the corporation that provided them with the compound HX4 investigated in the manuscript. All other authors declare no conflict of interest.

This article is a PNAS Direct Submission.

Freely available online through the PNAS open access option.

[1]To whom correspondence should be addressed. E-mail: ludwig.dubois@maastrichtuniversity.nl.

This article contains supporting information online at www.pnas.org/lookup/suppl/doi:10.1073/pnas.1102526108/-/DCSupplemental.

[^{18}F]HX4 would generate a suitable tumor-to-background signal ratio earlier compared with other established hypoxia markers. The aim of this study was to evaluate the in vivo uptake of [^{18}F]HX4 over time in an experimental rat tumor model by noninvasive PET imaging and to define the optimal imaging time point. Secondary aim was to validate the heterogeneity of the [^{18}F]HX4 accumulation by comparison with the exogenous hypoxia marker pimonidazole, and third aim was to establish a causal relationship between [^{18}F]HX4 uptake and tumor oxygenation.

Results

Synthesis and Metabolite Analysis. To increase the hydrophilicity of HX4, a metabolically stable 1,2,3-triazole compound was incorporated using the Cu-catalyzed Hüsigen click-chemistry reaction. Radiolabeling with fluorine-18 afforded [^{18}F]HX4 with a yield of 3–7 GBq [^{18}F]HX4 at the end of synthesis (14–35% decay-corrected yield) within 85 min total synthesis time. Radiochemical purity was higher than 95% and specific activity was typically in the area of 24 GBq/μmol. Calculation of the partition coefficients confirmed the hydrophilic character of HX4 [logP (octanol/water) = −0.69 ± 0.02 and logP(octanol/PBS) = −0.68 ± 0.01]. Radio-HPLC analysis showed that >90%, >85%, 60%, and 10% of plasma, urine, kidney, and liver radioactivity, respectively, represented intact [^{18}F]HX4 60 min after injection.

In Vivo Accumulation of [^{18}F]HX4 in an Experimental Rat Tumor Model. To evaluate the potential of [^{18}F]HX4 as a noninvasive marker of hypoxia, a clinically relevant (heterogeneous hypoxic pimonidazole-positive areas and low-percentage necrosis even at larger volumes) experimental rat rhabdomyosarcoma R1 tumor model (5, 11) was used at an average tumor volume of 12.894 ± 5.104 cm^3 (Fig. S1*A*). A clear heterogeneous accumulation of [^{18}F]HX4 was observed in the tumor (Fig. 1*B*), whereas equal [^{18}F]HX4 activity levels were found in surrounding normal tissues. Furthermore, a high accumulation of [^{18}F]HX4 was found in the bladder, confirming its renal clearance. Quantification of [^{18}F]HX4 accumulation was done by volume of interest (VOI) analysis of the heart, hind leg muscles, and tumor. The heart was selected as reference tissue to noninvasively analyze whole-blood ^{18}F activity, as previously shown (11). Mean [^{18}F]HX4 activity levels in tumor and muscle tissue were comparable ($P = 0.795$) during the first hour after injection (Fig. 1*C Left*), whereas the blood pool mean activity level was found to be significantly higher ($P < 0.0001$). Maximum activity levels showed a similar pattern (Fig. 1*C Right*). No significant differences were observed between mean and maximum activities in the blood pool ($P = 0.566$) and muscle ($P = 0.227$). However, maximum activity levels in tumors were significantly higher ($P = 0.0004$) compared with the corresponding mean accumulation. From 2 h after injection onward, a significantly ($P < 0.0001$) faster clearance of [^{18}F]HX4 from the blood and muscle was observed compared with the tumor (Table S1). This resulted in a significant ($P < 0.001$) increase in mean tumor-to-blood (T/B) ratios until 4 h after injection, where a mean T/B of 2.512 ± 0.578 was reached (Fig. 1*D Left*). No further increase was observed at later time points, making 4 h after injection an optimal time point for [^{18}F]HX4 evaluation in tumors. Because tumors are known to be heterogeneous, we also analyzed the maximum T/B signal ratios and found a similar pattern of increase, with a maximum of 7.638 ± 0.926 at 4 h post injection (Fig. 1*D Right*). A progressive clearance from normal tissues was observed because muscle-to-blood (M/B) ratios gradually decreased with time, resulting in significantly ($P < 0.05$) lower M/B ratios from 4 h post injection on. Both mean and maximum [^{18}F]HX4 uptake (percentage injected radioactivity per mL; %ID/mL) was independent of the tumor volume ($r^2 < 0.050$; $P > 0.4$) for all investigated time points.

Pimonidazole Staining, Hypoxic Fraction, and the Relationship with [^{18}F]HX4 Accumulation. To investigate the relationship between [^{18}F]HX4 accumulation and pimonidazole hypoxic fraction, taking into account the heterogeneity in uptake of both chemicals, tumors were divided into 16 pieces based on the computed tomography (CT) image according to their orthogonal planes (Fig. 2*A*). HX4 percentage injected dose, based on the PET image, was heterogeneously distributed across the tumor (Fig. 2 *A* and *B*) and ranged from 1 to 19%.

Pimonidazole-positive staining areas (range: 0.713–19.346 mm^2) were observed in all tumor pieces, with a heterogeneous distribution across the pieces (Fig. 2*C*). Staining was localized in most cases at a distance (several cell layers) from a perfused (Hoechst-positive) blood vessel, most often near areas of necrosis, indicative of diffusion-limited hypoxia (Fig. 2*D Lower*). However, there is also evidence for the presence of perfusion-limited hypoxia (Fig. 2*D Upper*), indicated by pimonidazole-positive staining in close proximity to perfusion marker-negative vessels. The hypoxic fraction ranged from 0.006 to 0.146 and was independent ($r = 0.152$; $P = 0.662$) of the tumor volume.

On whole-tumor level, a relationship between [^{18}F]HX4 accumulation and pimonidazole hypoxic fraction was observed ($r = 0.600$) but not significant ($P = 0.285$). On the other hand, on tumor-regional level, a strong and significant ($r = 0.722$; $P < 0.0001$) relationship (Fig. 2*E*) was observed between the hypoxic fractions as assessed using [^{18}F]HX4 noninvasive imaging and pimonidazole staining.

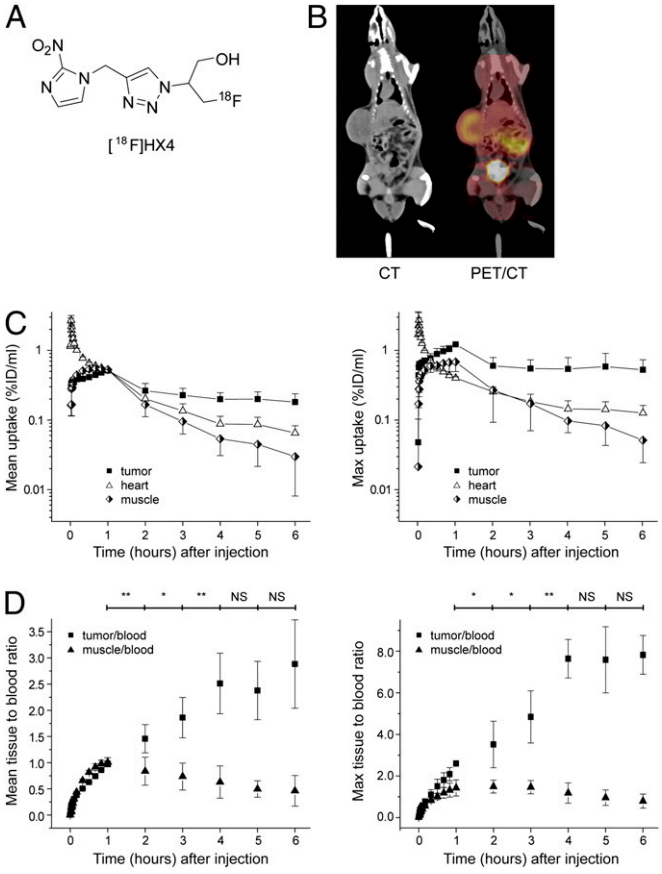

Fig. 1. Heterogeneous [^{18}F]HX4 accumulation occurs at optimal imaging properties 4 h after injection. (*A*) Structure of [^{18}F]HX4. (*B*) Representative CT and PET/CT image of a rhabdomyosarcoma R1 tumor-bearing rat 4 h after injection of [^{18}F]HX4. (*C*) Quantification of mean and maximum [^{18}F]HX4 uptake up to 6 h after injection. Uptake data ($n = 21$) for tumor (squares), heart (triangles), and muscles from the hind legs (diamonds) are shown and data are expressed as mean ± SD %ID/mL. (*D*) Mean and maximum tissue-to-blood ratios of [^{18}F]HX4 uptake up to 6 h after injection. Ratios represent tumor (squares) and muscle (triangles) uptake divided by blood pool uptake. Data are expressed as mean ± SD. Asterisks indicate significant increase in tumor-to-blood ratios between individual time points (*$P < 0.01$, **$P < 0.001$). NS, not significant.

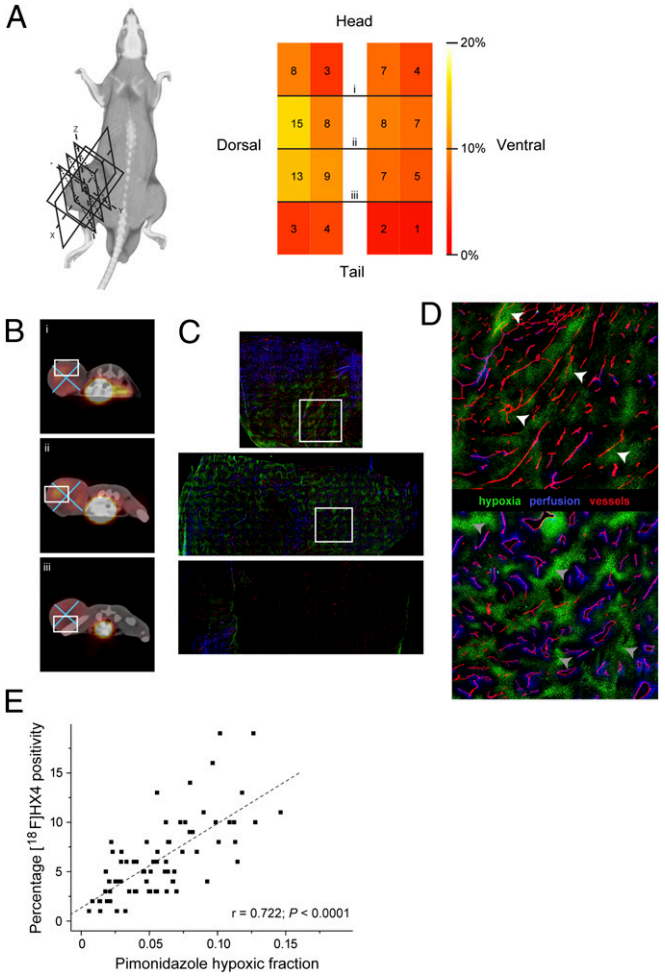

Fig. 2. [^{18}F]HX4 accumulation correlates with the hypoxic fraction of the tumors. (*A*) Division of the tumor into 16 pieces based on the CT image according to their coronal (XY), sagittal (XZ), and transaxial (YZ) planes at the largest diameter and quartiles. A representative heat map of the distribution of the percentage HX4 positivity is shown. (*B*) Representative axial PET/CT views of the mid and quartile axes of the heat map. (*C*) Pseudocolored gray-value images of the areas highlighted in the axial PET/CT views showing pimonidazole staining (green), vessels (red), and perfusion (blue). (*D*) Higher-magnification images of the areas highlighted in the original stainings. Areas of perfusion-limited (white) or diffusion-limited (gray) hypoxia are indicated with arrowheads. (*E*) Relationship at the regional level (n = 76) between [^{18}F]HX4 accumulation and pimonidazole hypoxic fraction.

[^{18}F]HX4 Accumulation Is Dependent on Available Oxygen. To test this hypothesis, we used two short-term treatments to modify tumor oxygenation. To increase or decrease tumor hypoxia, animals were exposed to an environment containing, respectively, 7% oxygen or a combination of nicotinamide and carbogen. No adverse effects were observed for either treatment regimen. First, a baseline [^{18}F]HX4 acquisition was performed on tumor-bearing (13.029 ± 5.149 cm^3) animals breathing normal air. Two days later (volume 15.882 ± 6.284 cm^3), animals were randomized into the two treatment groups and [^{18}F]HX4 accumulation was compared with the baseline uptake. Maximum [^{18}F]HX4 uptake at the optimal imaging time point in the same animal was found to be significantly lower (~40%; $P < 0.001$) after treatment with a combination of nicotinamide and carbogen (Fig. 3 *A* and *C*). This reduced accumulation persisted over time until 4 h after injection (Fig. S1*B Left*) and was lost at later time points. Also, the mean [^{18}F]HX4 uptake was significantly lower ($P < 0.01$) after treatment, but to a smaller extent (25%).

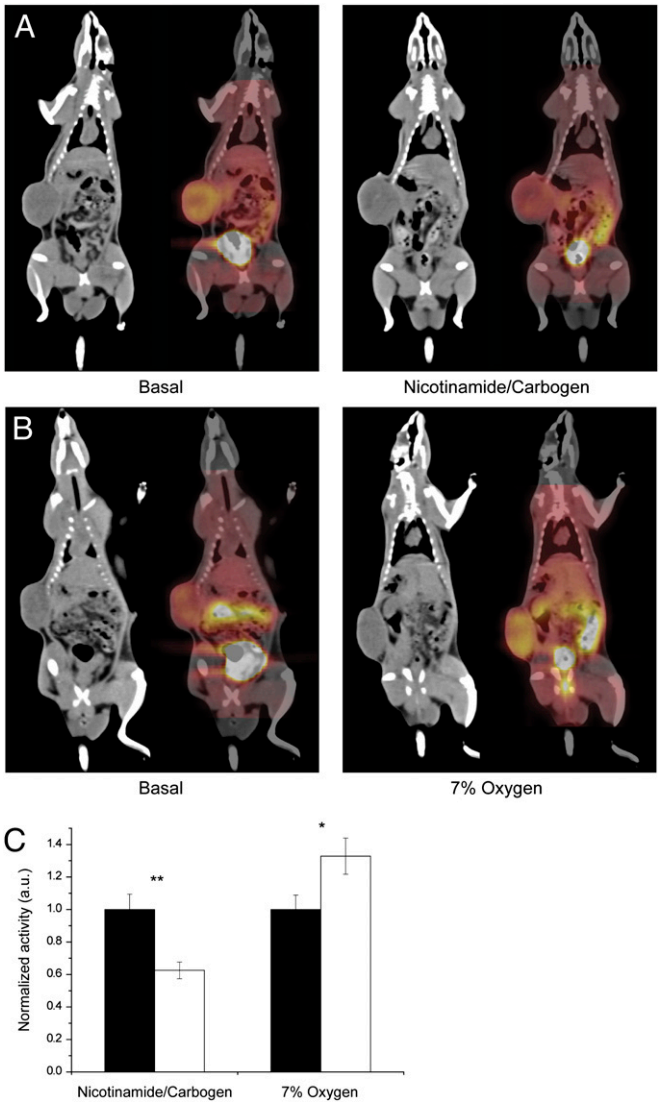

Fig. 3. [^{18}F]HX4 accumulation depends on tumor oxygenation. (*A* and *B*) Representative set of CT and PET/CT images within the same animal 4 h after injection of [^{18}F]HX4 before and after treatment (interval of 2 d) with (*A*) a combination of nicotinamide and carbogen or (*B*) 7% oxygen breathing. Images are scaled to the maximum-intensity values of all images. (*C*) Quantification of maximum [^{18}F]HX4 uptake in animals treated (white bars) with nicotinamide and carbogen (n = 7) or 7% oxygen breathing (n = 6) compared with no treatment (black bars) at the optimal imaging time point 4 h after injection. Data are expressed as mean ± SD. Asterisks indicate significant difference (*$P < 0.05$, **$P < 0.001$) compared with no treatment.

Furthermore, no significant differences in [^{18}F]HX4 accumulation were observed after treating the animals with a combination of nicotinamide and carbogen for blood and muscle tissue (Table S2), indicating that normal tissues can indeed cope with changes in oxygenation. On the other hand, when animals were treated with 7% oxygen, a significant increase (~30%; $P < 0.05$) in maximum [^{18}F]HX4 uptake in the tumor was observed (Fig. 3 *B* and *C*) persisting over time (Fig. S1*B Right*). The effect of 7% oxygen breathing on normal tissues was also negligible (Table S2). Evaluation of the mean [^{18}F]HX4 activity in the tumor after 7% oxygen treatment resulted in increased accumulation, but statistical significance was lost. Furthermore, also the mean and maximum [^{18}F]HX4 uptake after oxygen modification were independent ($r = 0.356$; $P > 0.3$ and $r = 0.368$; $P > 0.3$ for 7%

oxygen breathing or a combination of nicotinamide and carbogen, respectively) of the tumor volume.

Discussion

Increasing evidence points to an important role for tumor hypoxia in sensitivity to radio- and chemotherapy (9), indicating the necessity to evaluate oxygenation in individual tumors. Over the last decade, noninvasive methods that can identify tumors with substantial hypoxic fractions have been developed and may be used to acquire knowledge of the variations in spatial distribution of hypoxia (4). PET using the 2-nitroimidazole [^{18}F]FMISO holds promise for the evaluation of tumor hypoxia at both global and local levels. Several alternative nitroimidazole derivatives have been developed to overcome some of the limitations of [^{18}F]FMISO such as nonspecific retention, metabolic conversion, and low partition coefficient, all leading to faster clearance properties (8).

In the current study, we evaluated the in vivo oxygen-dependent uptake of [^{18}F]HX4, a novel 2-nitroimidazole nucleoside analog PET tracer, in a rat tumor model. The Cu-catalyzed Hüsigen click-chemistry reaction was used to incorporate a metabolically stable 1,2,3-triazole moiety, resulting in increased hydrophilicity of HX4 evidenced by the lower logP value (−0.69 ± 0.02) compared with FMISO (−0.40 ± 0.02), FAZA (0.04), and EF3 (0.05) (17–20). Unexpectedly, incorporation of the 1,2,3-triazole moiety improved the clearance properties relative to FMISO, demonstrating that kidney-bladder is the major HX4 excretion pathway (15) whereas FMISO clearance mainly occurs through the hepatobiliary and gastrointestinal pathway (Table S3). Additionally, when clearance shifts more toward the renal pathway, less metabolism is expected. Metabolite analysis showed >90%, >85%, 60%, and 10% intact [^{18}F]HX4 in plasma, urine, kidney, and liver, respectively. It should be noted that the percentage injected dose corrected for weight (%ID/g) of [^{18}F]HX4 in liver is <0.3% (15), indicating that the majority of [^{18}F]HX4 remained intact. For [^{18}F]FMISO the highest activity was found in liver and intestines (Table S3), and intact [^{18}F]FMISO in plasma, urine, kidney, and liver were 47%, 77%, 3%, and 3%, respectively (18). Our data strongly suggest that the hydrophilic [^{18}F]HX4, cleared through the kidneys, will result in a faster decrease of the background signal, leading to a larger imaging window and an increased biostability profile.

We observed a clear [^{18}F]HX4 accumulation in tumors compared with the surrounding normal tissue and a progressive decrease in concentration with time. A mean T/B ratio of 2.515 ± 0.578 was observed 4 h after injection, higher than the described cutoff value (T/B > 1.4) indicative for significant hypoxia obtained from [^{18}F]FMISO imaging of several human tumors (21). No further increase was observed at later time points, making 4 h after injection an optimal time point for [^{18}F]HX4 evaluation in tumors. A large heterogeneity in uptake, imaging time, and tumor and animal models for different hypoxia markers have been observed in the literature, making comparison hard to interpret. Table S4 provides a summary of animal studies with 2-nitroimidazole-based hypoxia markers [^{18}F]FMISO, [^{18}F]FAZA, [^{18}F]EF3, nitro-1H-imidazol-1-yl-N-[^{18}F]-pentafluoropropyl acetamide ([^{18}F]EF5) and [^{18}F]FETNIM (structures in Fig. S1*C*). Most studies have focused on [^{18}F]FMISO, and a broader range in T/B or T/M (tumor-to-muscle) ratios was observed for rodent (2.04–11) compared with human (1.28–5.7) tumor models. Also, imaging occurred relatively fast (2–3 h) after injection. For [^{18}F]FAZA, a similar broader range for rodent (2.9–9.82) as for human (2.0–6.1) tumor models was found, but at a later time (3 h). For the other hypoxia markers, no data are available on human tumor models, but a trend has been noticed for imaging at even later time points (3–5 h). Although characterization of new hypoxia markers should be preferably performed in multiple cancer models, highly additive data can be expected from comparisons of different tracers in the same tumor models. We found that [^{18}F]HX4 uptake in this rhabdomyosarcoma model was generally lower both in normal and in tumor tissue compared with previously reported [^{18}F]EF3 activities (11), resulting in comparable mean T/B ratios. As tumors are known to be heterogeneous, we also analyzed the maximum T/B uptake at 4 h post injection and observed an almost twofold increased T/B (7.638 ± 0.926) for [^{18}F]HX4 compared with [^{18}F]EF3 (4.84 ± 0.23) (11). This suggests that [^{18}F]HX4 in this model reflects better on tumor heterogeneity and the extent of hypoxia.

Heterogeneous patterns of [^{18}F]HX4 accumulation were seen across different tumor regions, as exemplified by high-count density regions in a rim of the tumor surrounding a central part of low radioactivity reflecting diffusion-limited hypoxia and regions with a hot spot distribution representing perfusion-limited hypoxia. Similar heterogeneous uptake patterns were previously observed for [^{18}F]FMISO and [^{18}F]EF3 in the same model (5, 11). Also, in other species bearing tumors, heterogeneous patterns of hypoxia marker accumulation have been observed. Imaging of [^{18}F]FMISO uptake in xenograft-bearing mice demonstrated both high focal and more patchy distribution of the hypoxia PET tracer (22). These heterogeneous patterns of accumulation can be explained by the way vascular structures, responsible for the tracer influx and washout, are organized within the tumor. Regions with strong [^{18}F]HX4 accumulation surrounding necrotic or normoxic areas receive their blood supply from vascular sheets, whereas regions demonstrating a more diffuse uptake are supplied from a central vessel (23). Microregional distribution of hypoxia was assessed using immunohistochemical staining of the bioreductive hypoxia marker pimonidazole, a compound known to give a reliable estimate of radiobiologically relevant hypoxia (24). A comparable pattern in heterogeneous staining was observed for pimonidazole, with evidence for the presence of both diffusion- and perfusion-limited hypoxia at a distance or in close proximity to vessels, respectively. Within tumor areas, a strong and significant correlation was observed between the percentage positivity for [^{18}F]HX4 and pimonidazole. The hypoxic fractions were used, because they have been shown to be a more robust parameter for tumor hypoxia than that based on intensity profiles (22). When heterogeneity was not taken into account, whole-tumor mean or maximum [^{18}F]HX4 accumulation was not significantly correlated with a pimonidazole-obtained hypoxic fraction. It has been shown that independent of the statistical methodology at least three, but preferably four or five tumor core biopsies from different tumor regions, are required to cover tumor heterogeneity (25). Ideally, to analyze microregional tumor heterogeneity, voxel-to-voxel analysis should be performed, but this is practically only feasible when autoradiography sections are available. Using this method, significant correlations between pimonidazole-obtained hypoxic fraction and [^{18}F]FMISO (22) and [^{18}F]FAZA (26) accumulation were observed.

Furthermore, a causal relationship was found between [^{18}F]HX4 accumulation and tumor oxygenation, because a significant reduction in uptake was observed within the same animal when [^{18}F]HX4 was injected after a treatment combining nicotinamide and carbogen. This combination treatment has been shown to reduce tumor hypoxia in both preclinical and clinical practice (27, 28). Carbogen breathing is known to reduce chronic hypoxia by increasing the oxygen diffusion distance, whereas nicotinamide prevents intermittent vascular shutdown, resulting in a reduction in perfusion-limited hypoxia (29, 30). Furthermore, [^{18}F]HX4 accumulated in tumors after 7% oxygen breathing, lending further support that HX4 acts as a sensitive and reversible tumor hypoxia marker in vivo. A similar increase in mean [^{18}F]FMISO intensity was observed in a glioblastoma model after clamping (22). The effect of the oxygen modification treatment persisted ∼4 h, in agreement with the observed decrease in [^{18}F]EF3 accumulation in FSA II tumor-bearing mice breathing carbogen (18). Although studies have investigated the oxygen dependence of several noninvasive hypoxia markers using autoradiography or biodistribution studies, only a few demonstrated this dependency using PET imaging. For example, [^{18}F]FMISO ratios of tumor to reference tissues significantly decreased upon

carbogen/oxygen breathing in different murine tumor models (27). Also, for serial animal [^{18}F]FAZA PET marker studies, a significant reduction in tumor-to-background ratios was obtained after breathing pure oxygen or carbogen (31, 32).

[^{18}F]HX4 biodistribution in normal tissues was found to be fast and homogeneous, as has already been published for [^{18}F]EF3 and [^{18}F]FMISO in the same rat model (11). The low uptake levels of [^{18}F]HX4 in intestines, liver, kidney, and other normal tissues result in lower background signals, providing good imaging properties. A progressive clearance was observed with time and the uptake in muscle was always lower than in the blood. [^{18}F]HX4 M/B ratios were comparable to [^{18}F]EF3 M/B ratios 2 h after injection, but whereas [^{18}F]EF3 ratios remained equal with time (11), [^{18}F]HX4 ratios decreased, indicating a faster clearance from normal tissues. This is in agreement with dosimetry data obtained in healthy humans 4 h after injection, where the absorbed doses for most organs were lower for [^{18}F]HX4 compared with [^{18}F]FMISO and [^{18}F]FETNIM, except for the kidneys and bladder (16). This is, however, not surprising, because the highest [^{18}F]HX4 uptake was found in the urinary bladder, confirming excretion primarily through the kidneys. To reduce bladder and kidney dose, patients should therefore be encouraged to maintain adequate hydration and void frequently (15, 16).

Our results demonstrate that noninvasive nuclear imaging of tumor oxygenation at a macroscopic level using [^{18}F]HX4 is possible and agrees with the overall hypoxic fraction. This indicates that [^{18}F]HX4 PET would be a valuable tool for therapy prediction and response evaluation. Pre-therapy [^{18}F]FMISO uptake has been shown to be an independent predictor for outcome in head and neck cancer patients (7), and [^{18}F]FMISO uptake patterns after therapy correlated well with the tumor response (6). Additionally, the well-established clearance properties of [^{18}F]FMISO appear to be minimally different between rodents and humans (33), and given that both [^{18}F]FMISO and [^{18}F]HX4 localize to hypoxic tissues as a result of the 2-nitroimidazole, the ability of [^{18}F]HX4 to perform similarly in humans is not an unreasonable prediction. This also suggests that the faster [^{18}F]HX4 clearance rates found in rodents would similarly apply to humans. The clinical applicability of [^{18}F]HX4 was demonstrated in a phase 1 study in NSCLC patients with no obvious toxicity (34). Furthermore, a heterogeneous [^{18}F]HX4 accumulation was observed (Fig. 4) with a substantial increase in T/M ratios in the second hour after injection. Because imaging was performed in end-stage patients and no optimal imaging time point could be defined, future clinical trials using [^{18}F]HX4 should investigate and explore (*i*) imaging at later time points, (*ii*) the capacity to evaluate and predict therapy response, and (*iii*) the possibility of applying dose painting or similar dose escalation strategies to hypoxic regions.

Conclusion

[^{18}F]HX4 has been shown to be a promising in vivo tracer for the noninvasive detection and evaluation of tumor hypoxia. Both in preclinical models as well as in patients, a heterogeneous [^{18}F]HX4 accumulation was observed with optimal imaging properties 4 h after injection and a strong dependency on tumor oxygenation. A strong significant correlation was found between [^{18}F]HX4 accumulation and the hypoxic fraction of the tumors as measured by pimonidazole staining. [^{18}F]HX4 retention in normal tissues was found to be short-lived, homogeneous and characterized by a progressive temporal clearance. Taken together, our results indicate that [^{18}F]HX4 is a good candidate for hypoxia assessment in vivo at a macroscopic level and may find clinical utility in image-guided and intensity-modulated radiotherapy applications.

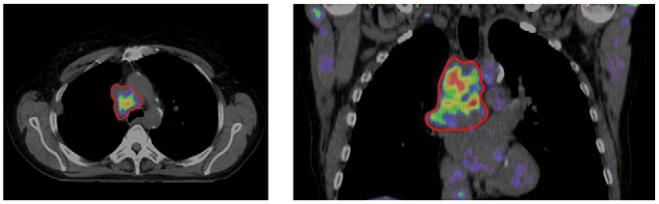

Fig. 4. Representative transaxial (*Left*) and coronal (*Right*) [^{18}F]HX4 PET/CT image of an NSCLC patient. [^{18}F]HX4 accumulation is shown within the gross tumor volume (GTV) delineated based on the CT image.

Materials and Methods

Animal and Tumor Model. All procedures and experiments were approved by the Animal Ethical Committee of the University of Maastricht (KdVR/ND 2008-135). Adult male WAG/Rij rats (275 ± 19 g) were implanted s.c. with syngeneic rhabdomyosarcomas (1-mm^3 R1 tumors) in the lateral flank. Experiments were started on average 42 d after transplantation, when tumors reached an average volume of 12.894 ± 5.104 cm^3 (Fig. S1*A*).

Synthesis and Metabolite Analysis. 3-[^{18}F]fluoro-2-(4-((2-nitro-1H-imidazol-1-yl)methyl)-1H-1,2,3-triazol-1-yl)propan-1-ol ([^{18}F]HX4; Fig. 1*A*) was synthesized from the precursor: 3-(formyloxy)-2-{4-[(2-nitro-1*H*-imidazol-1-yl) methyl]-1*H*-1,2,3-triazol-1-yl}propyl 2-nitrobenzenesulfonate (16) supplied by Siemens Molecular Imaging. [^{18}F]HX4 was obtained by nucleophilic substitution of 2-nitrobenzenesulfonate ester with [^{18}F]fluoride in acetonitrile/t-butanol with Kryptofix-2.2.2 and K_2CO_3 followed by acidic hydrolysis. The product was isolated from the crude reaction mixture by HPLC and reformulated into a sterile, isotonic, and pyrogen-free saline solution containing 7.09 mM sodium hydrogen phosphate and 10 mg/mL ascorbic acid. The product was stable in the formulation solution for at least 6 h at room temperature. Solutions of HX4 at 0.2–50 μg/mL were prepared in a mixture (1:9) of n-octanol and water or phosphate buffer (pH 7.4) to measure logP values. Samples (100 μL) from both phases were analyzed by HPLC (Phenomenex Gemini C18 column, 4.5 × 150 mm, flow 1 mL/min, UV 330 nm) for quantitative measurements. The percentages of intact HX4 in plasma, urine, kidney, and liver 60 min after injection were analyzed by HPLC.

Experimental Design. Before and during PET acquisition, rats were anesthetized with sodium pentobarbital (60 mg/kg, i.p.). The radiolabeled tracer was administered into a lateral tail vein via an i.v. line (Venoflux 0.4 mm G27) flushed with diluted heparin saline solution. Pretreatment with nicotinamide (500 mg/kg, i.p.), carbogen (95% O_2, 5% CO_2), and 7% oxygen (residual N_2) breathing occurred as previously described (14).

Rat Imaging Acquisition. Imaging was performed using a dedicated PET/CT Biograph scanner (SOMATOM TruePoint Sensation-40 with an ECAT ACCEL PET scanner; Siemens) with an axial field of view (FoV) of 162 mm, a transaxial FoV of 605 mm, and a spatial resolution of 5.3 mm FWHM at the center of the FoV. The acquired CT images were used for attenuation correction of the PET data. Also, corrections for scatter (3D), randoms, dead time, and decay of the injected radionuclides were applied. After acquiring a topogram, a whole-body CT scan was acquired using a 1-mm reconstructed slice thickness and a pitch of 0.8. Simultaneously with tracer injection (20.430 ± 2.418 MBq), a dynamic emission scan in list mode (LM) was started for 60 min in one bed position encompassing the heart, tumor, and hind legs of the rat. Afterward, LM data were rebinned using Fourier rebinning, and PET images were reconstructed as previously described (5). Two hours post injection, the rats were repositioned using external markers and a dedicated laser-positioning system (LAP) for a CT scan, immediately followed by a second dynamic emission scan performed for 20 min (rebinned into four frames of 5 min each). The same sequence was repeated each hour until 6 h after injection.

PET Image Analysis. The reconstructed PET/CT images were viewed and analyzed in dedicated software (TrueD VC60; Siemens). PET and CT images were automatically and rigidly registered based on a mutual information algorithm. Activity data (Bq/mL) in tumor, muscle, and blood pool (heart) were obtained by manual delineation of a VOI in the fused PET/CT images. All activity data were corrected for fluorine-18 decay toward injection time and, to minimize partial volume effects, recovery coefficients were calculated and applied to all of the data. Quantification of the data was done by calculation of the %ID/mL and T/B activity ratios. From the fused PET/CT images (for raw data see http://www.cancerdata.org), the tumors were divided based on the tumor contour manually drawn on the last time point CT image in 16 regions according to their coronal (XY), sagittal (XZ), and transaxial (YZ) planes at the largest diameter (Fig. 2*A*). The transaxial plane was further divided according to the quartiles. For each region, the total number of [^{18}F]HX4-

positive voxels (above background) was assessed and divided by the number of voxels in the tumor VOI to calculate the percentage [^{18}F]HX4 positivity.

Immunohistochemical Staining and Analysis. The exogenous hypoxia marker pimonidazole hydrochloride (PIMO; 60 mg/kg, i.p.) and the perfusion marker Hoechst 33342 (15 mg/kg, i.v.) were injected 1 h and immediately before euthanizing the animals, respectively. From each region, 5-μm sections were cut and mounted on poly-L-lysine-coated slides. After fixation in cold acetone, slides were scanned for fluorescent signal of Hoechst before staining for PIMO and vessels. Staining was done as previously described (22), using rabbit anti-pimonidazole (1:1,000; gift of J. A. Raleigh., University of North Carolina, NC) and goat anti-collagen IV (1:100; Southern Biotechnology Association). Grayscale images for each staining were obtained and converted into binary images. After thresholding above background staining for each individual marker, the hypoxic fraction represented as the ratio of the sum of all PIMO-positive pixels and the sum of all tumor pixels, including areas of necrosis, was calculated.

Statistics. All statistical analyses were performed with GraphPad Prism version 5.01 for Windows. An unpaired Student's *t* test and nonparametric Mann–Whitney *U* test for small groups were used to determine the statistical significance of differences between two independent groups of variables. Linear regression analysis was used to assess correlations (Spearman's *r*) between the different parameters. For all tests, $P < 0.05$ was considered significant.

ACKNOWLEDGMENTS. This work has been funded with the support of the European Union Seventh Framework Program (Metoxia Project 2008-222741), the Center for Translational Molecular Medicine (http://www.ctmm.nl) (AIRFORCE Project 030-103), and Siemens Molecular Imaging.

1. Nordsmark M, Overgaard J (2000) A confirmatory prognostic study on oxygenation status and loco-regional control in advanced head and neck squamous cell carcinoma treated by radiation therapy. *Radiother Oncol* 57:39–43.
2. Brown JM, Wilson WR (2004) Exploiting tumour hypoxia in cancer treatment. *Nat Rev Cancer* 4:437–447.
3. Tatum JL, et al. (2006) Hypoxia: Importance in tumor biology, noninvasive measurement by imaging, and value of its measurement in the management of cancer therapy. *Int J Radiat Biol* 82:699–757.
4. Ebbesen P, et al. (2009) Taking advantage of tumor cell adaptations to hypoxia for developing new tumor markers and treatment strategies. *J Enzyme Inhib Med Chem* 24(Suppl 1):1–39.
5. Dubois L, et al. (2004) Evaluation of hypoxia in an experimental rat tumour model by [(18)F]fluoromisonidazole PET and immunohistochemistry. *Br J Cancer* 91:1947–1954.
6. Gagel B, et al. (2006) [18F] Fluoromisonidazole and [18F] fluorodeoxyglucose positron emission tomography in response evaluation after chemo-/radiotherapy of non-small-cell lung cancer: A feasibility study. *BMC Cancer* 6:51.
7. Rajendran JG, et al. (2006) Tumor hypoxia imaging with [F-18] fluoromisonidazole positron emission tomography in head and neck cancer. *Clin Cancer Res* 12:5435–5441.
8. Krohn KA, Link JM, Mason RP (2008) Molecular imaging of hypoxia. *J Nucl Med* 49(Suppl 2):129S–148S.
9. Lucignani G (2008) PET imaging with hypoxia tracers: A must in radiation therapy. *Eur J Nucl Med Mol Imaging* 35:838–842.
10. Serganova I, Humm J, Ling C, Blasberg R (2006) Tumor hypoxia imaging. *Clin Cancer Res* 12:5260–5264.
11. Dubois L, et al. (2009) [18F]EF3 is not superior to [18F]FMISO for PET-based hypoxia evaluation as measured in a rat rhabdomyosarcoma tumour model. *Eur J Nucl Med Mol Imaging* 36:209–218.
12. Dehdashti F, et al. (2003) In vivo assessment of tumor hypoxia in lung cancer with 60Cu-ATSM. *Eur J Nucl Med Mol Imaging* 30:844–850.
13. Yuan H, et al. (2006) Intertumoral differences in hypoxia selectivity of the PET imaging agent 64Cu(II)-diacetyl-bis(N4-methylthiosemicarbazone). *J Nucl Med* 47: 989–998.
14. Dubois L, et al. (2009) Imaging of CA IX with fluorescent labelled sulfonamides distinguishes hypoxic and (re)-oxygenated cells in a xenograft tumour model. *Radiother Oncol* 92:423–428.
15. Walsh JC, Kolb HC (2010) Applications of click chemistry in radiopharmaceutical development. *Chimia (Aarau)* 64:29–33.
16. Doss M, et al. (2010) Biodistribution and radiation dosimetry of the hypoxia marker 18F-HX4 in monkeys and humans determined by using whole-body PET/CT. *Nucl Med Commun* 31:1016–1024.
17. Grunbaum Z, et al. (1987) Synthesis and characterization of congeners of misonidazole for imaging hypoxia. *J Nucl Med* 28:68–75.
18. Mahy P, et al. (2008) Comparative pharmacokinetics, biodistribution, metabolism and hypoxia-dependent uptake of [18F]-EF3 and [18F]-MISO in rodent tumor models. *Radiother Oncol* 89:353–360.
19. Mahy P, et al. (2004) Preclinical validation of the hypoxia tracer 2-(2-nitroimidazol-1-yl)- N-(3,3,3-[(18)F]trifluoropropyl)acetamide, [(18)F]EF3. *Eur J Nucl Med Mol Imaging* 31:1263–1272.
20. Sorger D, et al. (2003) [18F]Fluoroazomycinarabinofuranoside (18FAZA) and [18F] fluoromisonidazole (18FMISO): A comparative study of their selective uptake in hypoxic cells and PET imaging in experimental rat tumors. *Nucl Med Biol* 30:317–326.
21. Koh WJ, et al. (1992) Imaging of hypoxia in human tumors with [F-18]fluoromisonidazole. *Int J Radiat Oncol Biol Phys* 22:199–212.
22. Troost EG, et al. (2006) Imaging hypoxia after oxygenation-modification: Comparing [18F]FMISO autoradiography with pimonidazole immunohistochemistry in human xenograft tumors. *Radiother Oncol* 80:157–164.
23. Ljungkvist ASE, et al. (2002) Vascular architecture, hypoxia, and proliferation in first-generation xenografts of human head-and-neck squamous cell carcinomas. *Int J Radiat Oncol Biol Phys* 54:215–228.
24. Raleigh JA, Chou SC, Arteel GE, Horsman MR (1999) Comparisons among pimonidazole binding, oxygen electrode measurements, and radiation response in C3H mouse tumors. *Radiat Res* 151:580–589.
25. Goethals L, et al. (2006) A new approach to the validation of tissue microarrays. *J Pathol* 208:607–614.
26. Busk M, et al. (2009) Can hypoxia-PET map hypoxic cell density heterogeneity accurately in an animal tumor model at a clinically obtainable image contrast? *Radiother Oncol* 92:429–436.
27. Bentzen L, et al. (2002) Assessment of hypoxia in experimental mice tumours by [18F] fluoromisonidazole PET and pO2 electrode measurements. Influence of tumour volume and carbogen breathing. *Acta Oncol* 41:304–312.
28. Kaanders JH, et al. (1998) Accelerated radiotherapy with carbogen and nicotinamide (ARCON) for laryngeal cancer. *Radiother Oncol* 48:115–122.
29. Chaplin DJ, Horsman MR, Trotter MJ (1990) Effect of nicotinamide on the microregional heterogeneity of oxygen delivery within a murine tumor. *J Natl Cancer Inst* 82:672–676.
30. Powell ME, Hill SA, Saunders MI, Hoskin PJ, Chaplin DJ (1996) Effect of carbogen breathing on tumour microregional blood flow in humans. *Radiother Oncol* 41: 225–231.
31. Piert M, et al. (2005) Hypoxia-specific tumor imaging with 18F-fluoroazomycin arabinoside. *J Nucl Med* 46:106–113.
32. Reischl G, et al. (2007) Imaging of tumor hypoxia with [124I]IAZA in comparison with [18F]FMISO and [18F]FAZA—First small animal PET results. *J Pharm Pharm Sci* 10: 203–211.
33. Lee ST, Scott AM (2007) Hypoxia positron emission tomography imaging with 18F-fluoromisonidazole. *Semin Nucl Med* 37:451–461.
34. van Loon J, et al. (2010) PET imaging of hypoxia using [18F]HX4: A phase I trial. *Eur J Nucl Med Mol Imaging* 37:1663–1668.